ROYAL SOCIETY
OF CHEMISTRY

PAPER

Check for updates

Construction of an MXene/MIL Fe-53/ZIF-67 derived bifunctional electrocatalyst for efficient overall water splitting†

Komal Farooq,[a] Maida Murtaza,[a] Laraib Kiran,[a] Kashf Farooq,[b] Waqas Ali Shah [ID] *[a] and Amir Waseem [ID] *[a]

Research on water splitting is paramount for developing low-carbon alternative energy sources. Nevertheless, creating an efficient, cost-effective, and bifunctional electrocatalyst that facilitates both the oxygen evolution reaction (OER) and the hydrogen evolution reaction (HER) remains an elusive goal. In this work, we report a novel hybrid nanostructured electrocatalyst by combining and pyrolyzing MXene, MIL-53(Fe), and ZIF-67. Comprehensive characterization of the synthesized nanocomposites was conducted using XRD, FESEM, TEM, EDX, and XPS. Notably, among the synthesized electrocatalysts, M3 demonstrated exceptional performance, achieving 10 mA cm^{-2} at 237 mV and 50 mA cm^{-2} at 292 mV for the OER, and 10 mA cm^{-2} at 307 mV and 50 mA cm^{-2} at 481 mV for the HER. The Tafel slope values were 64 mV dec^{-1} for the OER and 185 mV dec^{-1} for the HER at 10 mA cm^{-2}. Moreover, M3 exhibited excellent stability, with negligible current density loss over 12 hours, and showed good mass activity of 57.5 and 54.6 A g^{-1} and TOFs of 1.56 and 2.97 s^{-1}, for the OER and HER, respectively. This study highlights the efficacy of integrating MXene (Ti$_3$C$_2$T$_x$) with MIL-53(Fe) and ZIF-67, creating a potent bifunctional OER and HER electrocatalyst. The synergistic combination enhances electrical conductivity, active site availability, and structural stability, yielding superior performance. The findings of this investigation underscore the importance of strategic design and optimization of bifunctional electrocatalysts for energy conversion applications.

1. Introduction

The widespread use of conventional energy systems, which are heavily dependent on finite fossil fuels, poses significant threats to global energy sustainability and environmental well-being.[1,2] Remarkable advancements in renewable energy conversion technologies are driving a paradigm shift towards a more sustainable, environmentally responsible, and energy-secure future. These innovations encompass water electrolysis, fuel cell systems, and metal-air energy storage.[3–5] Water splitting, which involves both hydrogen and oxygen evolution, is an exciting prospect for generating renewable energy in an environmentally responsible and sustainable manner. A crucial step in this process is the oxygen evolution reaction (OER: H$_2$O → O$_2$), which, despite its importance, suffers from relatively slow kinetics due to its intricate multistep proton-coupled electron transfer mechanism. Consequently, the development of a highly efficient and reliable electrocatalyst with minimal

overpotential remains a significant challenge to overcome. Addressing this issue is essential to enhance the viability of water splitting as a sustainable energy solution. IrO$_2$, RuO$_2$, and Pt/C are renowned noble metal-based catalysts, delivering exceptional oxygen evolution reaction (OER) and hydrogen evolution reaction (HER) performance. However, their widespread adoption is hindered by significant challenges, including poor long-term stability, prohibitive costs, and limited earth abundance. To address these limitations, the development of competent and affordable noble metal free electrocatalysts for the OER and HER is urgently needed.[6,7]

MXenes are two-dimensional (2D) materials consisting of transition metals combined with nitrides, carbides, or carbonitrides. They have a flat, layered structure similar to graphene, with a transition metal core that provides unique electronic and magnetic properties. The carbide, nitride, or carbonitride composition contributes to the material's chemical and physical characteristics.[8] On the other hand, metal–organic frameworks (MOFs) are crystalline polymeric materials composed of metal ions connected to organic ligands, exhibiting high surface areas due to their highly tunable porosity.[9] Their potential in water splitting applications has sparked widespread research interest.[10–12] The use of MXene and MOFs

[a]Department of Chemistry, Quaid-i-Azam University, Islamabad-45320, Pakistan. E-mail: amir@qau.edu.pk; waqaslishah1@hotmail.com

[b]Department of Chemistry, University of Poonch, Rawalakot, Azad Kashmir, Pakistan

synergistically exploits the unique advantages of each material, resulting in improved characteristics and performance.[13,14]

Zeolite Imidazolate Frameworks (ZIFs) are a unique subclass of MOFs characterized by their zeolite-like structure and composition. They consist of imidazole linkers and metal ions (typically zinc, cobalt, or copper). MXenes/ZIF hybrids have given rise to groundbreaking hybrid materials, attracting considerable attention for their diverse applications. These composites leverage the synergistic benefits of MXene and ZIF properties, yielding innovative materials with enhanced functionality.[15]

ZIF-67, a cobalt-based material, comprising imidazole molecules and Co(II) cations, forms a vigorous framework with a rigid pore network and exceptional thermal stability. This architecture enables ZIF-67 to exhibit a high specific surface area and enhanced oxidation reaction activity sites, making it an optimal precursor for advanced electrode materials.[16]

Another class of iron-based MOFs, abbreviated as MIL (Materials from Institute Lavoisier), have gained prominence due to their exceptional stability, mechanical strength, and industrial applicability.[17,18] MIL-53 (Fe) is formed through the assembly of infinite chains of corner-sharing $[FeO_4(OH/F)_2]$ or $[FeO_6]$ octahedra, linked by 1,4-benzene dicarboxylate (BDC) molecules. This configuration gives rise to a 3D network architecture featuring 1D channels aligned parallel to the inorganic backbone, forming a unique porous structure. A distinctive feature of MIL-53(Fe) is its malleable structure and adoptive pore size, allowing it to expand and accommodate guest molecules.[19]

Previous studies have shown that MOFs' catalytic performance can be enhanced by hybridizing them with other MOFs or two-dimensional materials.[20] Chen et al. constructed a hybrid ZIF-67/MIL-88(Fe, Ni) nanostructure. Co-M-Fe/Ni (150) performed remarkably in the OER and HER, with low overpotentials of 269 mV and 149 mV. The enhanced performance arises from the cooperative synergy between ZIF-67 and MIL-88(Fe, Ni), enhancing charge transfer and electrolyte penetration.[21] Pan et al. fabricated a hybrid nanostructure consisting of CoP nanoparticles integrated into nitrogen-doped carbon nanotube hollow polyhedra (NCNHP), obtained by sequential pyrolysis, oxidation, and phosphidation of ZIF-8@ZIF-67. The CoP/NCNHP hybrid demonstrated excellent bifunctional catalytic performance, requiring only 1.64 V to reach 10 mA cm^{-2} for the OER and 140 mV to reach 10 mA cm^{-2} for the HER, maintaining stability for 36 hours with minimal degradation.[22] Yuwen et al. reported a facile synthesis of trimetallic carbon nanoflowers derived from adjustable $Co^{2+}/Fe^{2+}/Ni^{2+}$ MOFs, exhibiting enhanced electrocatalytic performance resulting from the augmented surface area and synergistic effects between metals, which promote oxygen vacancies and carbon graphitization. The optimized $Co_{0.2}Fe_{0.8}$Ni-OCNF electrocatalyst demonstrates exceptional performance, delivering 10 mA cm^{-2} at a remarkably low overpotential of 291 mV for the OER and 259 mV to achieve −10 mA cm^{-2} for the HER.[23] Luo et al. reported a bimetallic Co–Ni MOF electrocatalyst on iron foam, exhibiting superior OER activity compared to monometallic counterparts, reaching 10 mA cm^{-2} at 264 mV overpotential in 0.1 M KOH.[24]

Our present investigation demonstrates the fabrication of Ti$_3$C$_2$T$_x$/MIL-Fe-53/ZIF-67, a novel hybrid nanocomposite combining MXene (Ti$_3$C$_2$T$_x$) with ZIF-67 and MIL-Fe-53 MOFs. This integration harnesses the exceptional properties of its components, including MXene's superb electrical conductivity, hydrophilicity, mechanical resilience, and flexibility, as well as ZIF-67's optimal topology and active cobalt sites, and MIL-53(Fe)'s stability and ion channels. The synergistic combination creates a robust electronic interface, enhancing catalytic activity through cooperative interactions and tailored electronic properties. Designed to optimize OER and HER performance, this hybrid nanocomposite shows promise for energy applications.

2. Experimental section

Details on materials, characterization methods, and electrochemical experiments can be found in the ESI.†

2.1 Preparation of MXene

To obtain MXene (Ti$_3$C$_2$T$_x$) from the MAX phase (Ti$_3$AlC$_2$), aluminum (Al) was etched using 2 g of Ti$_3$AlC$_2$ powder, which was gradually added to 50 mL of hydrofluoric acid (HF) and stirred constantly for 24 hours at 25 °C. The resulting suspension underwent repeated cycles of washing and centrifugation using deionized water until a neutral pH was reached. The final product was then dried in an oven at 70 °C for 24 hours[25] (Scheme S1†).

2.2 Synthesis of MXene/MIL Fe-53

To delaminate MXene into nanosheets, 0.2 g of MXene powder was sonicated in 36 mL of N,N-dimethylformamide (DMF) for 12 hours at 25 °C. The resulting MXene dispersion was then mixed with 1.08 g of ferric chloride hexahydrate (FeCl$_3$·6H$_2$O) and 0.77 g of 2-aminoterephthalic acid (NH$_2$-BDC) and stirred magnetically at 25 °C for 3 hours. The mixture was subsequently heated in an autoclave at 150 °C for 24 hours. After cooling, the product was washed with DMF and methanol repeatedly three times and oven-dried overnight at 60 °C (Scheme S2†). For comparison, MIL-Fe-53 was also synthesized separately using the same procedure without the addition of MXene.

2.3 Preparation of ZIF-67

A 0.1 M Co(NO$_3$)$_2$·6H$_2$O solution was mixed with a 0.8 M 2-methylimidazole solution in methanol solvent. The mixture was stirred magnetically for 3 hours at 25 °C, yielding a suspension. After repeated washing and centrifugation with ethanol to remove impurities, the resulting purified product, ZIF-67, was oven-dried overnight at 80 °C (Scheme S3†).

2.4 Preparation of the MXene/MIL Fe-53/ZIF-67 composite

A 50 mg sample of MXene/MIL-53(Fe) was dispersed uniformly in 60 mL of DMF and stirred magnetically for 30 minutes to make a homogeneous suspension. Variable amounts of ZIF-67

(50 mg, 100 mg, and 200 mg) were then added separately and sequentially to create three distinct samples. The mixtures were stirred at room temperature for 6 hours. Following repeated cycles of washing and centrifugation with DMF and methanol, the resulting purified samples were oven-dried thoroughly at 60 °C for 24 hours (Scheme S4†).

After drying, the samples were transferred to a ceramic boat and calcined in a tube furnace at 800 °C for 8 hours (ramping at 5 °C min^{-1}). The resulting materials were designated as M1, M2, and M3.

3. Results and discussion

3.1 Characterizations of catalysts

Fig. S1† shows the powder X-ray diffraction (XRD) pattern of MAX (Ti_3AlC_2) and MXene ($Ti_3C_2T_x$). The shifting and broadening of the diffraction peak at the 002 plane in $Ti_3C_2T_x$ confirm the exfoliation and etching of the MAX phase as reported previously.[26] Successful elimination of the Al from the MAX phase is further confirmed by the disappearance of the prominent peak at 104 planes in $Ti_3C_2T_x$. Upon the extraction of the Al layer from the MAX phase, a decrease in peak intensity also suggests the loss of crystallinity.[27]
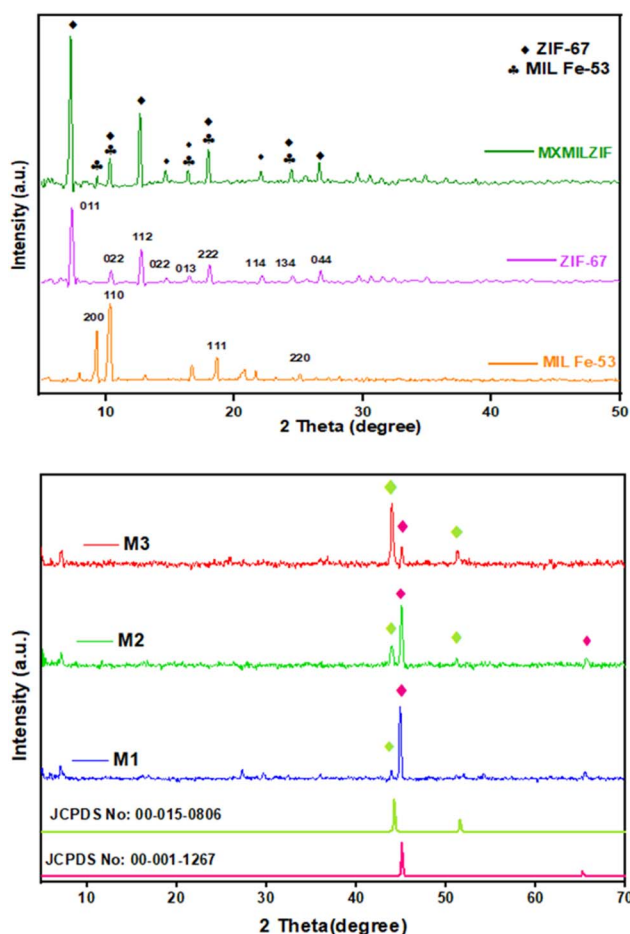
Fig. 1a confirms the successful preparation of MIL Fe-53 with prominent characteristic peaks at $2\theta = 9.38°$, $10.5°$, $18.3°$ and $25.2°$ similar to previous findings.[28] Fig. 1a shows the synthesized ZIF-67 XRD pattern, which exhibits peaks at $2\theta = 7.49°$, $10.52°$, $12.87°$, $14.82°$, $16.57°$, $18.17°$, $22.27°$, $24.62°$ and $26.81°$, in agreement with earlier findings.[29] The XRD pattern of MXMILZIF shows the characteristic peaks of MIL Fe-53 and ZIF-67. The overlapping of diffraction peaks suggests the successful integration of the two MOFs to form a composite material. The MXene in the composite is incorporated but no clear peaks for MXene are specifically marked due to the overlap or suppression of the MXene's diffraction peaks with those of ZIF-67 at $2\theta = 7.49°$. The effective production of the composite containing MXene, MIL Fe-53, and ZIF-67 is further confirmed by SEM, TEM, EDX and XPS analysis.

Fig. 1b shows the X-ray diffraction pattern of three calcined samples containing varying amounts of ZIF-67, labelled as M1, M2 and M3. All the peaks of the samples are in agreement with the cobalt and iron standard patterns, having the JCPDS card numbers 00-015-0806 and 00-001-1267, confirming the decomposition of the samples into relevant metals upon calcination.[30,31] The small and broad signal below 10° (2θ) shows the presence of $Ti_3C_2T_x$, which confirms that all samples contain MXene. Few other weak signals are also observed, which indicate the presence of TiO_2, possibly originating from surface oxidation during calcination. As the ZIF-67 content increases from M1 to M3, the cobalt peak becomes more prominent, as expected. The peaks are sharper and more intense in M3, indicating increased crystallinity.

FESEM was employed to examine the morphological features of the synthesized samples. Fig. 2a exhibits the characteristic layered structure of MXene, where stacked and sheet-like layers are clearly visible, which is similar to reported literature.[32] Fig. 2b shows the morphology of MIL Fe-53, which appears as cuboid small densely packed particles.[33] Fig. 2c displays ZIF-67 as a combination of tetragonal and cubic forms, which is in agreement with existing literature.[34,35] The SEM image (Fig. 2d) of the MXene/MIL Fe-53 composite shows a rough and agglomerated structure, which reveals that MXene sheets are covered with MIL Fe-53 particles, forming a heterogeneous structure. Fig. 2e shows the FESEM image of the composite material containing MXene (Ti_3C_2), MIL Fe-53 and ZIF-67. The surface is irregular and rough, with visible particles of varying sizes attached to the MXene layer, which suggests the successful combination of the three materials.

The calcined samples of the composite material with varying ZIF-67 contents (50, 100, and 200 mg) are displayed in Fig. 2f–h, denoted as M1, M2, and M3, respectively. The particles appeared to be uniformly dispersed across the surface. M1 shows well-defined crystals with finer dispersion, while M3 represents larger clusters. As the amount of ZIF-67 increases from M1 to M3, the particles become more aggregated, increasing the surface roughness.

Energy Dispersive X-ray (EDX) spectroscopy was employed for elemental analysis and quantification of the prepared samples, with results presented in Fig. S2.† The EDX spectra confirm the presence of Co, Fe, C, Ti, and O in M1, M2, and M3,

Fig. 1 (a) XRD patterns of MIL Fe-53, ZIF-67 and the MXMILZIF composite; (b) XRD patterns of M1, M2 and M3 composites.
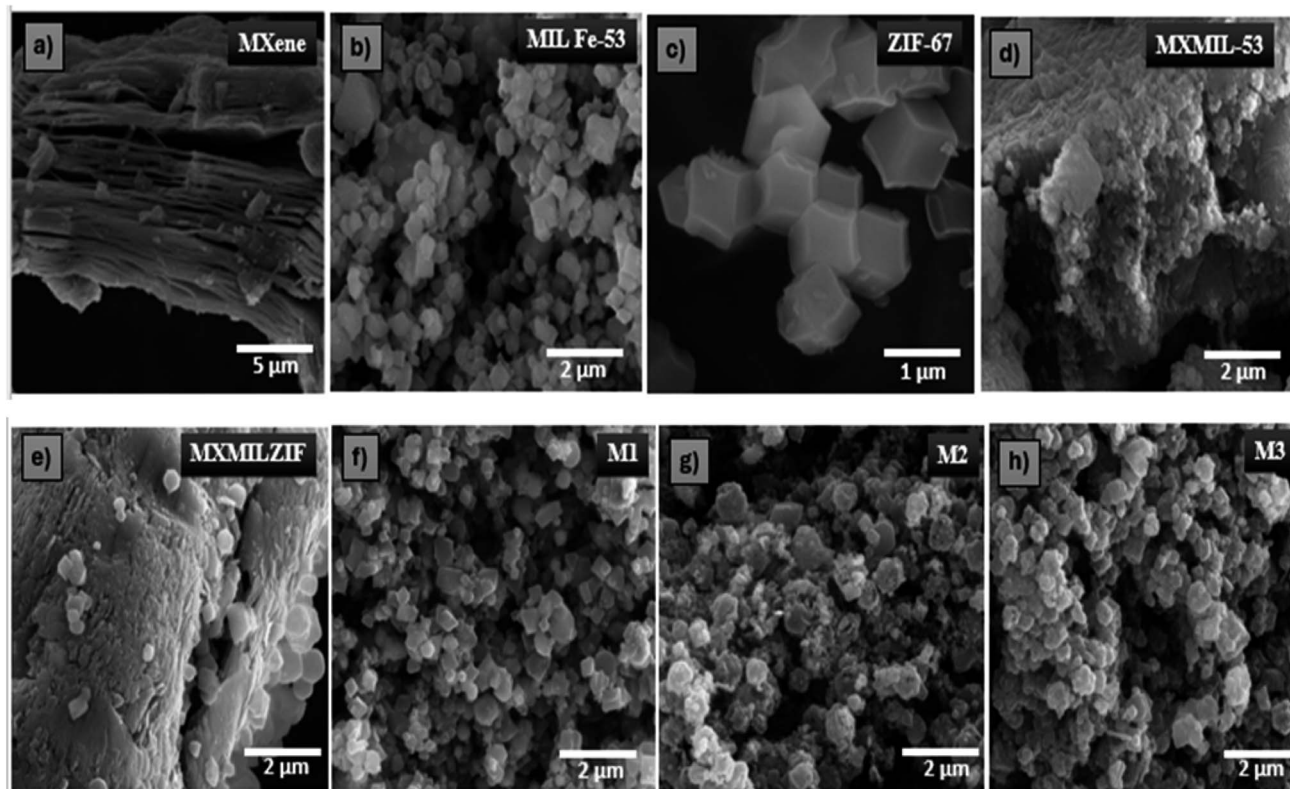
Fig. 2 FESEM images of (a) MXene, (b) MIL Fe-53, (c) ZIF-67, (d) MXMIL-53, (e) MXMILZIF, (f) M1, (g) M2 and (h) M3.

indicating successful synthesis. The EDX spectrum shows that M3 has a higher cobalt content with 42.7 wt%, while M1 and M2 have lower cobalt levels with 29.8 wt% and 39.9 wt%. The presence of titanium in all three samples suggests that the composite formed successfully.

Fig. 3 displays the high-resolution transmission electron microscopy (HRTEM) images of the M3 sample at 100, 20 and 5 nm along with corresponding elemental mapping. Fig. 3a shows the aggregated structure composed of small particles distributed across the field of view. These clusters contain nanoparticles that are composed of MXene sheets and calcined phases of MIL Fe-53 and ZIF-67. The darker regions, indicating higher electron density, are more likely MXene, while the lighter regions, more porous and less dense, may belong to calcined MIL Fe-53, ZIF-67 or the amorphous porous carbon matrix.[36] The spherical or irregular particles are visible as dark contrasts in Fig. 3b and c, at high resolution, which shows the presence of metal species (Co and Fe). The calcined material, with its porous nature, is distributed throughout the composite, forming the lighter regions and indicating uniform distribution. To further elucidate the composition, elemental mapping was done to visualize elemental distribution in the composite. Fig. 3d shows that all the elements including Co, Fe, Ti, C, O and N display analogous mapping patterns with the selected area of the TEM image.

To investigate the chemical composition and redox states of the M3 composite, X-ray Photoelectron Spectroscopy (XPS) was employed. Fig. 4a displays the survey scan that exhibits the existence of cobalt, iron, titanium, carbon, oxygen and nitrogen elements in the sample. In Fig. 4b, the peak of Co 2p shows spin–orbit splitting into Co $2p_{3/2}$ and Co $2p_{1/2}$. The Co $2p_{3/2}$ peak was deconvoluted into peaks at binding energies of 778.4 and 780.5 eV, which correspond to Co metal and CoO_x. The peaks located at binding energies of 796.6 and 802.3 eV represent the Co $2p_{1/2}$ and satellite peaks, respectively.[30] The Fe 2p XPS spectrum (Fig. 4c) exhibits two prominent peaks corresponding to Fe $2p_{1/2}$ (722.1 eV) and Fe $2p_{3/2}$ (713 eV), paired with two satellite peaks at 726 eV and 717 eV. Meanwhile, the peaks at binding energies of 710.5 and 705 eV correspond to metallic iron and FeO_x as reported previously.[33,37] The Ti 2p spectrum was identified as Ti $2p_{3/2}$ and Ti $2p_{1/2}$, which are assigned to TiO_x due to surface oxidation of $Ti_3C_2T_x$ MXene (Fig. 4d).[38] In the fine XPS spectrum of C 1s, the dominant peak around 284.5 eV originates from graphitic carbon with sp^2 or sp^3 hybridization. The peak at 285.7 eV is characteristic of a carbon atom bonded to nitrogen (C–N),[39] while the peak at 287.2 eV represents the C=O species.[35] XPS analysis of O 1s and N 1s spectra (Fig. 4f) indicates the occurrence of O–C, O=C, O–M, N–M, pyridinic N, and graphitic N species. The binding energies at 532.5, 531.5, and 529.5 eV correspond to O–C, O=C, and O–M, while the N 1s peaks at 397.6, 398.9, and 400.1 eV represent N–M, pyridinic N, and graphitic N.[38]

3.2 Electrochemical studies

The OER was electrochemically investigated employing linear sweep voltammetry (LSV) within a potential window of 0–1.5 V
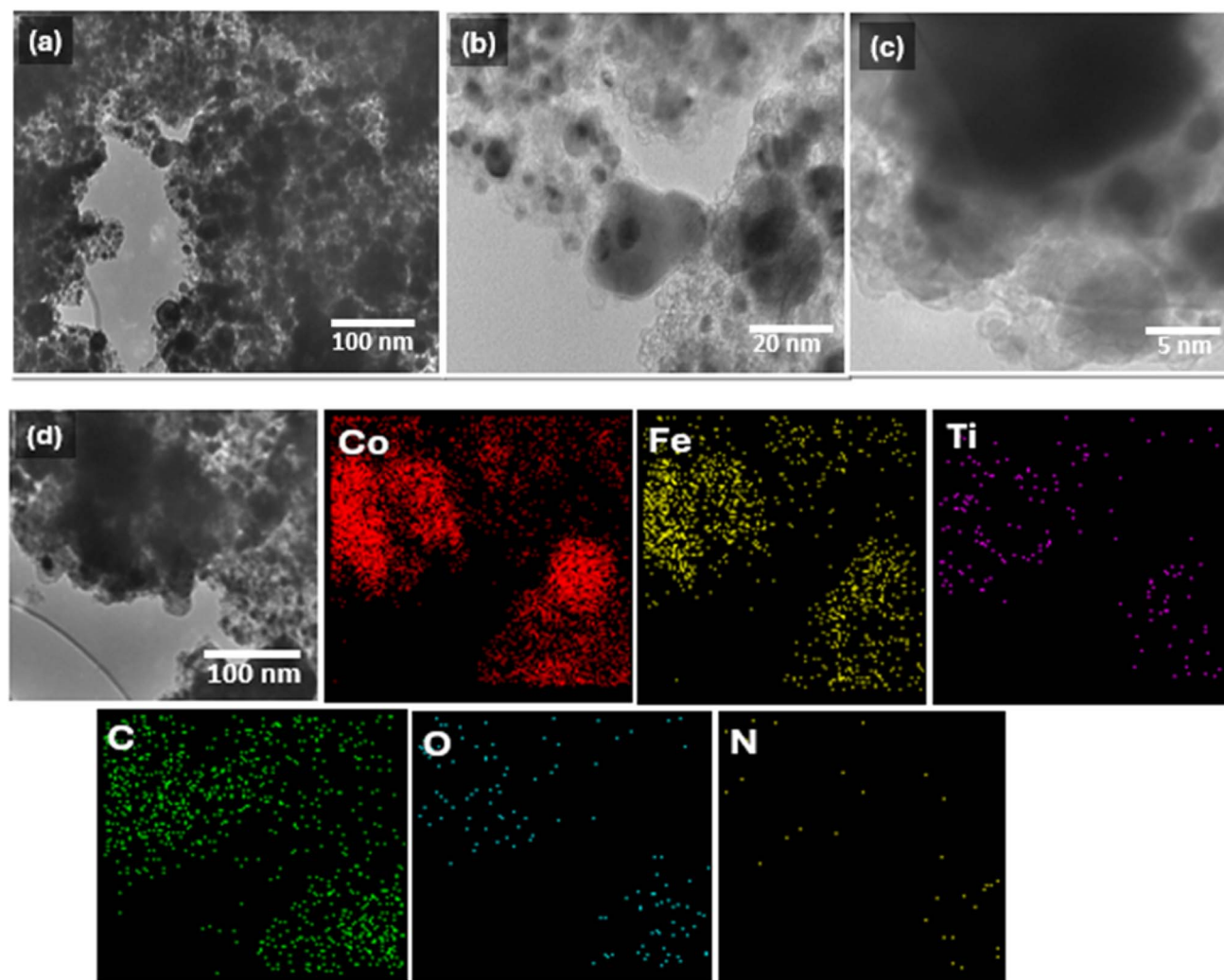
Fig. 3 TEM images of the M3 catalyst (scale bar: (a) 100 nm, (b) 20 nm and (c) 5 nm); (d) elemental mapping of the M3 catalyst.

at a scan rate of 5 mV s^{-1}. Experiments were performed in oxygen-saturated 1 M KOH, engaging a Hg/HgO as the reference electrode. The LSV curves of RuO$_2$, M1, M2 and M3 are shown in Fig. 5a. The onset potentials and current densities were 1.42 V, 1.46 V, and 1.50 V, and j_{max} values (mA cm^{-2}) were 160, 159, and 130 mA cm^{-2} for M3, M2, and M1, respectively. A comparison of the overpotential at 10 mA cm^{-2} from the LSV curves reveals that the sample M3 displays a markedly reduced overpotential of 237 mV at 10 mA cm^{-2}, outperforming M1 (299 mV), M2 (271 mV), and RuO$_2$ (331 mV) at the same current density. M3 achieves a current density of 50 mA cm^{-2} at a remarkably low overpotential of 292 mV for the OER, indicating relatively superior OER activity. The comparison of η_{10} values of the prepared samples is presented in the form of a bar graph in Fig. 5b. Tafel slope measurements were conducted to elucidate the kinetics of the OER. Fig. 5c reveals that M3 presents a significantly lower Tafel slope of 64 mV dec^{-1}, compared to M1 (73 mV dec^{-1}), M2 (121 mV dec^{-1}), and RuO$_2$ (139 mV dec^{-1}). These values further confirm the superior catalytic behavior of the M3 catalyst for the OER, as smaller Tafel slope values indicate higher electrocatalytic activity and fast kinetics.

These results indicate that the combination of MXene and MOFs (ZIF-67 and MIL-53) can significantly lower the overpotential required for water oxidation by facilitating faster electron transfer, thus improving the overall efficiency for the water oxidation process.

The electrocatalytic activity was further probed using electrochemical impedance spectroscopy (EIS), conducted in the non-faradaic region over a frequency of 10^2 to 10^6 Hz range. Fig. 5d presents the Nyquist plots with real and imaginary components of EIS, where M3 reveals the smallest semicircle, signifying the lowest charge transfer resistance. This also validates the material's unique combination of a high surface area, conductivity, and charge transfer efficiency.

To assess catalytic efficiency, the electrochemically active surface area (ECSA) was evaluated by measuring the double layer capacitance (C_{dl}) using cyclic voltammetry (CV) scans. CV scans were executed in the non-faradaic region from 10 to 100 mV s^{-1} scan rates (Fig. S3†). From the CV scans, the anodic current density variation was linearly correlated with the scan rate at a given voltage to get the value of C_{dl}. The ECSA values were calculated by normalizing the double layer capacitance
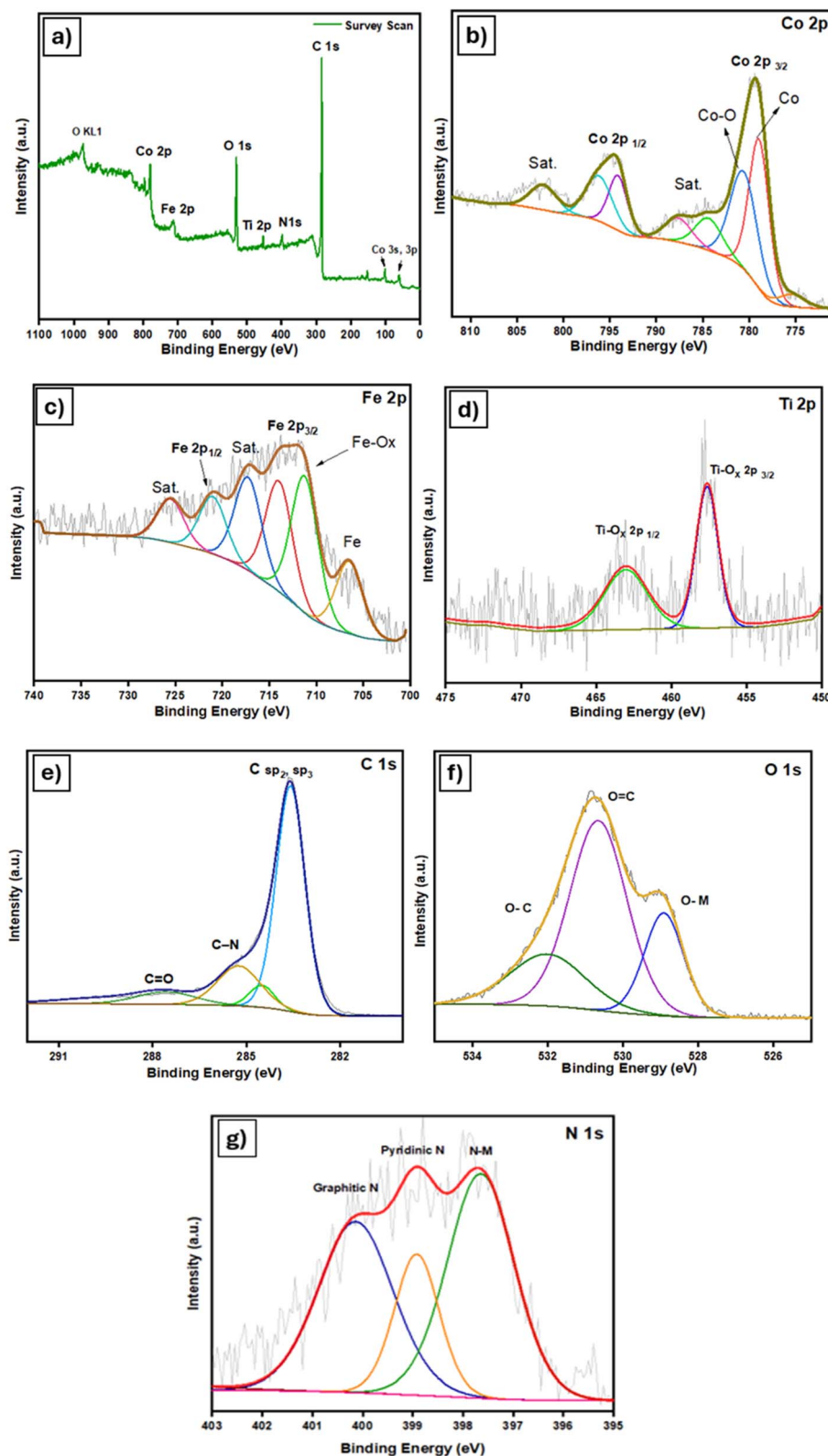
Fig. 4 High-resolution XPS spectra of (a) survey scan of M3, (b) Co 2p, (c) Fe 2p, (d) Ti 2p, (e) C 1s, (f) O 1s and (g) N 1s.

(C_{dl}) and the specific capacitance (C_s) of the electrolyte, assumed to be 0.02 mF cm^{-2}. Table S1† shows the C_{dl} and ECSA values of the synthesized catalysts. The results show that M3 has a greater C_{dl} value of 1.15 mF cm^{-2} among all the catalysts and

thus possesses a higher electrochemically active surface area (ECSA), which is 57.5 cm^2. Another surface feature that is crucial to the electrode material's electrocatalytic activity is the roughness factor (R_f), which can be computed using the

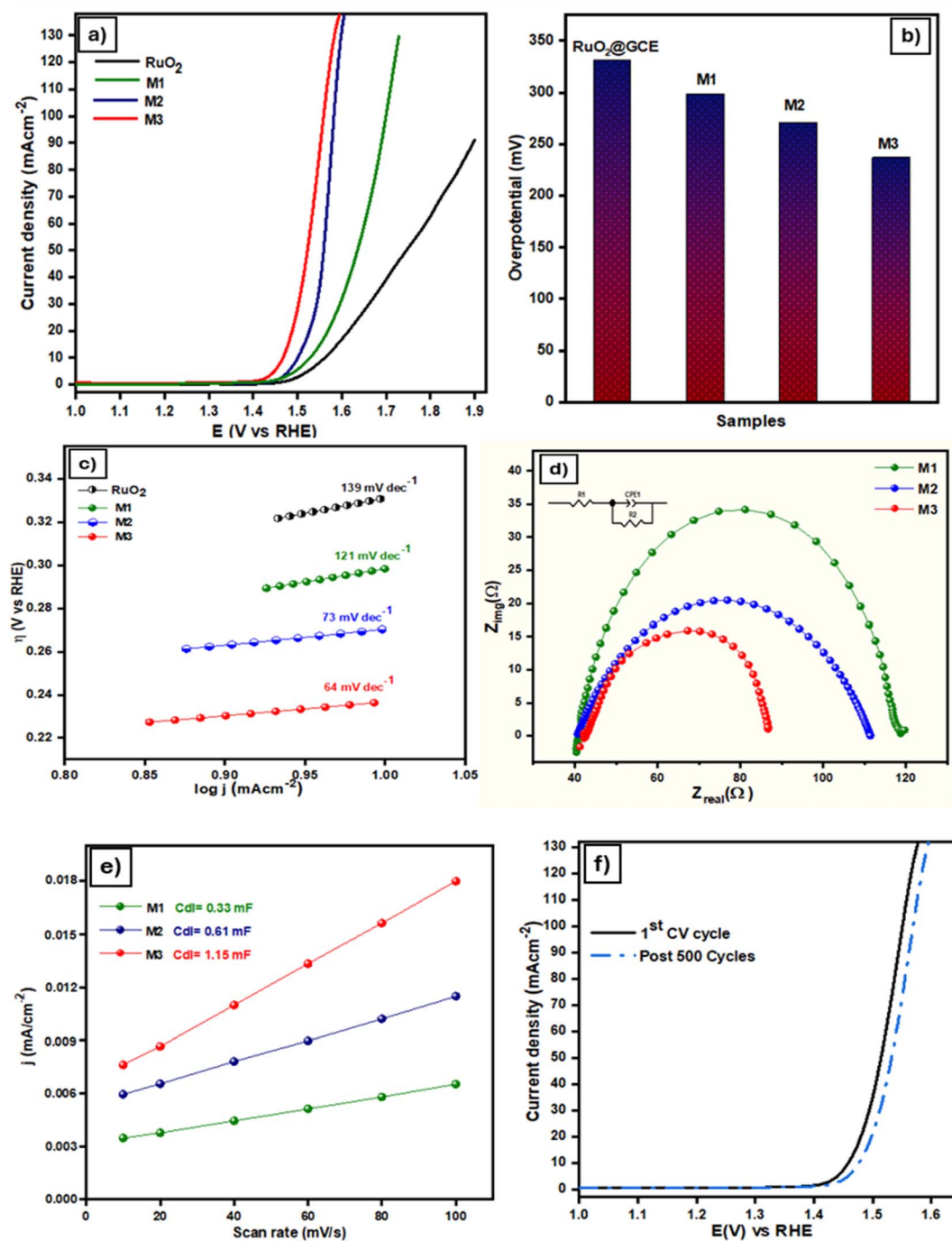© 2025 The Author(s). Published by the Royal Society of Chemistry

Fig. 5 Electrocatalytic OER performance: (a) OER LSV curves, (b) OER overpotential comparison of the prepared samples in a bar graph, (c) Tafel slope, (d) electrochemical impedance spectroscopy (EIS), (e) double layer capacitance (C_{dl}) graph and (f) LSV curves of M3 before and after 500 CV cycles.

electrode's geometric area divided by the ECSA. The higher R_f value of M3 (821.4) among all catalysts further confirms the improved electrochemical OER activity.

The robustness of the catalyst was assessed through chronoamperometry measurements conducted at 1.60 V *vs.* RHE in 1 M KOH electrolyte for a duration of 12 hours. As shown in Fig. S4† initially there is a slight decrease in current density from around 70 mA cm^{-2}, which then stabilizes after a few hours and remains relatively constant throughout the 12 hour

test. This indicates the strong electrochemical stability and durability of the catalyst in an extended chronoamperometry test, with minimal degradation, confirming its high stability. Fig. 5f shows the LSV curves observed before and after 500 CV cycles, indicating no major difference, thus further confirming the high stability of the catalyst.

The LSV curves for the HER of the products and the commercial reference sample 20% Pt/C are shown in Fig. 6a. HER performance was assessed in a three-electrode
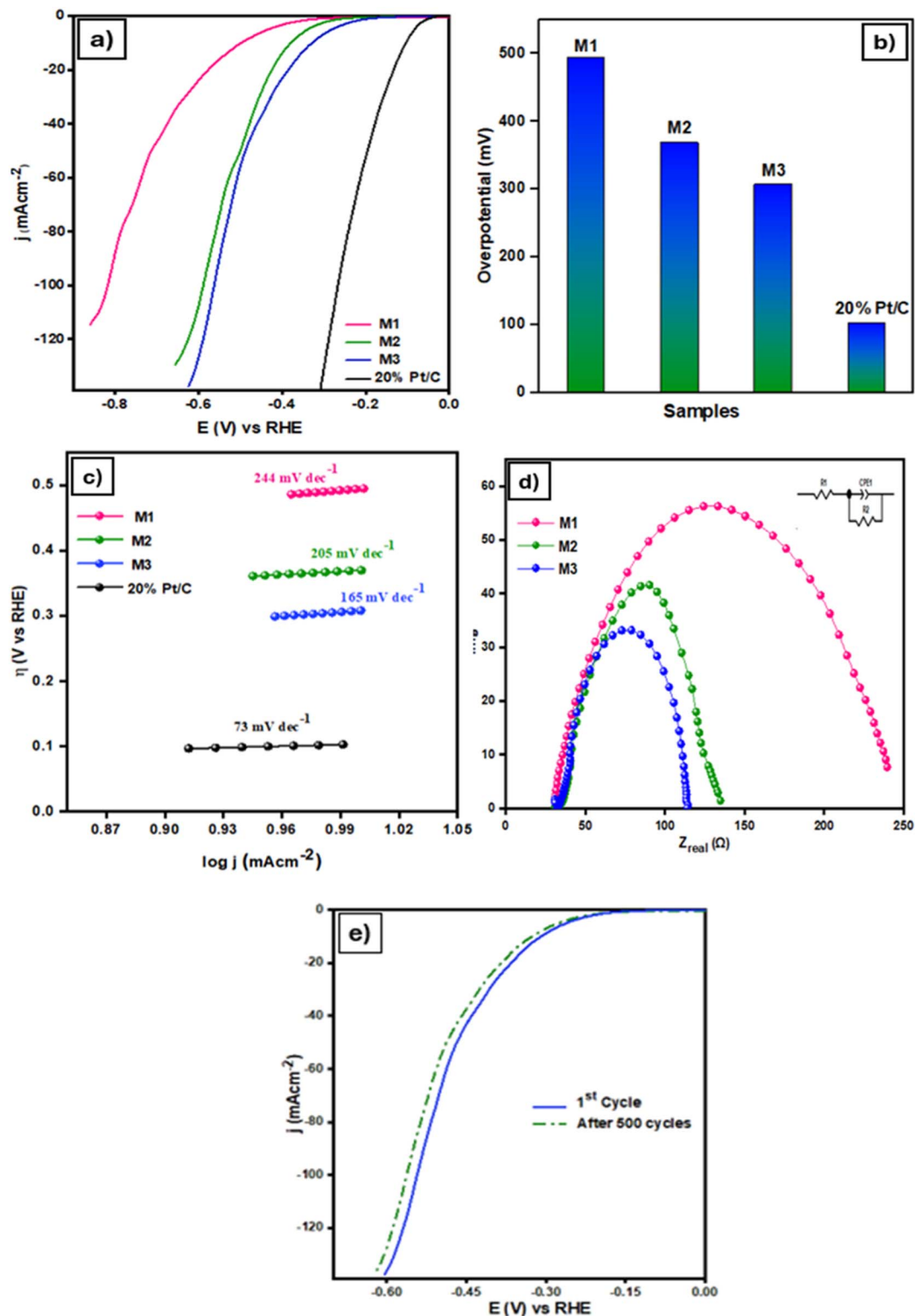
Fig. 6   HER electrocatalytic performance: (a) LSV curves, (b) HER overpotential comparison bar graph of the prepared samples, (c) Tafel slope, (d) electrochemical impedance spectroscopy (EIS), and (e) LSV curves of M3 before and after 500 CV cycles.

configuration with 0.5 M H_2SO_4 electrolyte. The commercial 20% Pt/C catalyst demonstrated exceptional activity, requiring an overpotential of only 103 mV to achieve -10 mA cm^{-2}, consistent with literature reports [A]. The sample M3 (MXene/

MIL Fe-53/ZIF-67@200) exhibits the lowest η_{10} and superior HER activity compared to M1 and M2. The overpotential values required to reach -10 mA cm^{-2} for M1, M2, and M3 are 494 mV, 369 mV, and 307 mV, respectively. Notably, M3 achieves an

overpotential of 481 mV at -50 mA cm^{-2}. Fig. 6b presents a comparative bar graph of η_{10} values for the catalysts. The Tafel slope values are displayed in Fig. 6c, where 20% Pt/C shows the lowest slope of 78 mV dec^{-1}. Among the synthesized catalysts, M3 has the lowest Tafel slope of 185 mV dec^{-1}, outperforming M1 (244 mV dec^{-1}) and M2 (205 mV dec^{-1}). In comparison to M1 and M2, the catalyst M3, which has the largest ZIF-67 loading (200 mg), exhibits the strongest HER performance, achieving the desired current density of -10 mA cm^{-2} at a lower overpotential. This implies that a greater ZIF-67 content increases the composite's HER activity, while lower ZIF-67 levels (50 mg and 100 mg, respectively) in M1 and M2 result in lower HER activity and larger overpotentials required to achieve the same current density. EIS was conducted to investigate the electron transfer properties of the catalysts. As depicted in Fig. 6d, among the catalysts tested in the EIS experiment, the catalyst M3 has the lowest charge transfer resistance (R_{ct}), confirming a rapid interfacial charge transfer between the electrode and the electrolyte. Fig. 6e proves the stability of M3 for the HER over 500 cycles. The polarization curves for the 1st cycle and after 500 cycles are nearly identical, indicating minimal performance degradation. This stability suggests strong durability and robustness of the catalyst for the HER.

The superior electrocatalytic activity of M3 in the OER and HER is likely due to the high density of Co active sites provided by the increased ZIF-67 content, promoting efficient proton adsorption and hydrogen generation. By using Co nanoparticles to form a porous carbon structure, pyrolyzed ZIF-67 enhances electron transport and catalyst–electrolyte interaction. With increased ZIF-67 levels in M3, conductivity and stability are optimized using MXene and MIL-53(Fe). This synergy between the active areas and conductive support provides enhanced OER and HER electrochemical activities.

Tables S2 and S3† show the OER and HER activities in terms of overpotential, Tafel slope values, mass activities, and turnover frequencies (TOF) for the reported catalysts. The mass activity at $\eta = 0.250$ V of 57.5 and 54.6 A g^{-1}, for the OER and HER, respectively, was found for M3, outperforming other studied catalysts (Tables S2 and S3†). The intrinsic activities of the above catalysts were further estimated from turnover frequencies (TOFs), assuming every metal atom to be catalytically active.[40] M3 shows the highest TOF values of 1.56 and 2.97 s^{-1} at $\eta = 0.350$ V for the OER and HER, respectively, which are quite higher than those of the M1 and M2 catalysts (Tables S2 and S3†)

The exceptional electrocatalytic activity of the desired electrocatalyst (M3), which is formed by the combination of titanium carbide MXene along with metal–organic frameworks (MOFs) such as ZIF-67 and MIL Fe-53, may be attributed to the following:

(a) 2D transition metal carbides, known as MXenes, exhibit great promise for electrocatalytic applications due to their exceptional conductivity, hydrophilic properties, and large surface area. Because of their metallic conductivity, MXenes can improve the catalytic performance by increasing the efficiency of charge transfer. Additionally, MXenes endow the composite

with mechanical strength and structural stability, inhibiting the active sites' deterioration during prolonged application.

(b) MIL Fe-53 is a highly porous and flexible MOF, which may serve as a structural stabilizer and enhance the accessibility of active sites, thus facilitating ion transport and enhancing the overall efficiency of the electrochemical process.

(c) ZIF-67, a cobalt-based MOF with a zeolite-inspired structure, boasts numerous active sites accessible through its porous architecture, thereby enhancing catalytic activity. However, its intrinsic conductivity limitations are alleviated by integration with MXene.

Thus, the combination of MXene with ZIF-67 and MIL Fe-53 enhances electrical conductivity, increases active site exposure, improves stability, and boosts catalytic activity for the OER and HER, resulting in lower overpotential and higher current density. Table S4† shows the OER and HER overpotentials at a current density of 10 mA cm^{-2} from reported literature and it was observed that the as-prepared catalysts show impressive performance compared to previous studies.

4. Conclusion

This study demonstrates the successful preparation of a high-performance durable electrocatalyst for water splitting through pyrolysis of MXene Ti$_3$C$_2$T$_x$-supported MOFs (MIL-53(Fe) and ZIF-67). The negatively charged Ti$_3$C$_2$T$_x$ MXene surface effectively anchors MOFs, preventing aggregation and promoting stability. MIL Fe-53 and ZIF-67 have a highly porous framework and large surface area, which improve charge transfer efficiency across the electrocatalyst, boosting efficiency and productivity in the OER and HER. MXenes provide high electrical conductivity for rapid electron transfer, chemical stability for enhanced catalyst durability, and versatile surface functionalization (–OH and –F) to strengthen interactions with MIL-53(Fe) and ZIF-67, improving stability and integration in the composite. This work indicates that combining 2D MXene with MOFs can unleash enhanced functional capabilities by utilizing the compositional and morphological flexibility of 2D materials. This research opens up a new avenue for rational design of high efficiency bifunctional electrocatalysts for energy transformation and storage applications.

Data availability

The data supporting this article have been included as part of the ESI.†

Conflicts of interest

There are no conflicts to declare.

Acknowledgements

References

1 Q. Zhou, J. Feng, X. Peng, L. Zhong and R. Sun, Porous Carbon Coupled with an Interlaced MoP–MoS₂ Heterojunction Hybrid for Efficient Hydrogen Evolution Reaction, *J. Energy Chem.*, 2020, **45**, 45–51.

2 B. Zhu, G. Yang, D. Gao, Y. Wu, J. Zhao, Y. Fu and S. Ma, Special Atmosphere Annealed Co₃O₄ Porous Nanoclusters with Oxygen Defects and High Proportion of Co²⁺ for Oxygen Evolution Reaction, *J. Alloys Compd.*, 2019, **806**, 163–169.

3 P. Li, M. Wang, X. Duan, L. Zheng, X. Cheng, Y. Zhang, Y. Kuang, Y. Li, Q. Ma and Z. Feng, Boosting Oxygen Evolution of Single-Atomic Ruthenium through Electronic Coupling with Cobalt-Iron Layered Double Hydroxides, *Nat. Commun.*, 2019, **10**, 1711.

4 S. Zaman, X. Tian, Y.-Q. Su, W. Cai, Y. Yan, R. Qi, A. I. Douka, S. Chen, B. You and H. Liu, Direct Integration of Ultralow-Platinum Alloy into Nanocarbon Architectures for Efficient Oxygen Reduction in Fuel Cells, *Sci. Bull.*, 2021, **66**(21), 2207–2216.

5 S. Zaman, Y. Q. Su, C. L. Dong, R. Qi, L. Huang, Y. Qin, Y. C. Huang, F. M. Li, B. You and W. Guo, Scalable Molten Salt Synthesis of Platinum Alloys Planted in Metal–Nitrogen–Graphene for Efficient Oxygen Reduction, *Angew. Chem., Int. Ed.*, 2022, **61**(6), e202115835.

6 A. Areeb Amjad, M. Murtaza, S. Shoaib Ahmad Shah, I. Ahmad, H. Alawadhi, W. Ali Shah and A. Waseem, Atomically Precise MOF-Based Electrocatalysts by Design: Hydrogen Evolution Applications, *Fuel*, 2025, **385**, 134021.

7 S. Zaman, M. Khalid and S. Shahgaldi, Advanced Electrocatalyst Supports for Proton Exchange Membrane Water Electrolyzers, *ACS Energy Lett.*, 2024, **9**, 2922–2935.

8 K. Hantanasirisakul and Y. Gogotsi, Electronic and Optical Properties of 2d Transition Metal Carbides and Nitrides (Mxenes), *MXenes*, 2023, 135–205.

9 W. A. Shah, S. Mir, S. Abbas, S. Ibrahim, L. Noureen, A. Kondinski, D. R. Turner, P. Kögerler and M. A. Nadeem, Robust and Efficient Electrocatalyst for Water Oxidation Based on 4,4′-Oxybis (Benzoate)-Linked Copper(II) Hydroxido Layers, *Inorg. Chim. Acta*, 2019, **497**, 119080.

10 X.-K. Wang, J. Liu, L. Zhang, L.-Z. Dong, S.-L. Li, Y.-H. Kan, D.-S. Li and Y.-Q. Lan, Monometallic Catalytic Models Hosted in Stable Metal–Organic Frameworks for Tunable CO₂ Photoreduction, *ACS Catal.*, 2019, **9**(3), 1726–1732.

11 S. Ibrahim, M. M. Saleem, M. Imran, W. A. Shah, D. B. Cordes, A. M. Slawin and M. A. Nadeem, A Two-Dimensional Manganese-Containing Coordination Polymer for Efficient Catalysis of the Oxygen Evolution, *Inorg. Chim. Acta*, 2022, **539**, 121030.

12 S. Ibrahim, U. Rafique, M. Saleem, W. Iqbal, S. Abbas, W. A. Shah, M. Imran and M. A. Nadeem, High Performance of Homo-Metallic Tetracyanonickelate Based Coordination Polymer Towards Water Oxidation Electrocatalysis, *Inorg. Chim. Acta*, 2021, **526**, 120510.

13 M. Murtaza, K. Farooq, W. A. Shah, I. Ahmad and A. Waseem, Layered MOF Supported on 2d Delaminated Mxene (Mo₂Ti₂C₃) Nanosheets Boosted Water Splitting, *Nanoscale Adv.*, 2024, **6**, 6317–6327.

14 M. Murtaza, L. Saleem, W. A. Shah, I. Ahmad, H. Alawadhi and A. Waseem, Delaminated Vanadium Carbide Mxene Supported Two-Dimensional (2D) CoNH₂BDC MOF Hybrid for Enhanced Water Splitting, *Ind. Eng. Chem. Res.*, 2024, **63**(48), 20915–20924.

15 K. S. Ranjith, S. Sonwal, A. Mohammadi, G. S. R. Raju, M.-H. Oh, Y. S. Huh and Y.-K. Han, Imparting Hydrophobicity to a MOF on Layered Mxene for the Selective, Rapid, and ppb Level Humidity-Independent Detection of NH₃ at Room Temperature, *J. Mater. Chem. A*, 2024, **12**(38), 26132–26146.

16 S. Iravani, E. N. Zare, A. Zarrabi, A. Khosravi and P. Makvandi, Mxene/Zeolitic Imidazolate Framework (ZIF) Composites: A Perspective on Their Emerging Applications, *FlatChem*, 2024, **44**, 100631.

17 W. A. Shah, A. Waseem, M. A. Nadeem and P. Kögerler, Leaching-Free Encapsulation of Cobalt-Polyoxotungstates in MIL-100 (Fe) for Highly Reproducible Photocatalytic Water Oxidation, *Appl. Catal., A*, 2018, **567**, 132–138.

18 W. A. Shah, S. M. Abbas, M. Adil, S. Ibrahim, Q. A. Bhatti and S. Li, Catalytic Efficiency and Kinetic Analysis of Manganese Polyoxometalate Heterogenized in MIL-100-Fe for Selective Olefin Oxidation Using H₂O₂, *Mol. Catal.*, 2024, **567**, 114456.

19 F. Millange, N. Guillou, M. E. Medina, G. Férey, A. Carlin-Sinclair, K. M. Golden and R. I. Walton, Selective Sorption of Organic Molecules by the Flexible Porous Hybrid Metal–Organic Framework MIL-53 (Fe) Controlled by Various Host–Guest Interactions, *Chem. Mater.*, 2010, **22**(14), 4237–4245.

20 W. A. Shah, S. Ibrahim, S. Abbas, L. Naureen, M. Batool, M. Imran and M. A. Nadeem, Nickel Containing Polyoxometalates Incorporated in Two Different Metal-Organic Frameworks for Hydrogen Evolution Reaction, *J. Environ. Chem. Eng.*, 2021, **9**(5), 106004.

21 P. Chen, X. Duan, G. Li, X. Qiu, S. Wang, Y. Huang, A. Stavitskaya and H. Jiang, Construction of ZIF-67/MIL-88 (Fe, Ni) Catalysts as a Novel Platform for Efficient Overall Water Splitting, *Int. J. Hydrogen Energy*, 2023, **48**(20), 7170–7180.

22 Y. Pan, K. Sun, S. Liu, X. Cao, K. Wu, W.-C. Cheong, Z. Chen, Y. Wang, Y. Li and Y. Liu, Core–Shell ZIF-8@ ZIF-67-Derived Cop Nanoparticle-Embedded N-Doped Carbon Nanotube Hollow Polyhedron for Efficient Overall Water Splitting, *J. Am. Chem. Soc.*, 2018, **140**(7), 2610–2618.

23 Y. Li, M. Lu, Y. Wu, H. Xu, J. Gao and J. Yao, Trimetallic Metal–Organic Framework Derived Carbon-Based Nanoflower Electrocatalysts for Efficient Overall Water Splitting, *Adv. Mater. Interfaces*, 2019, **6**(12), 1900290.

24 P. Luo, S. Li, Y. Zhao, G. Ye, C. Wei, Y. Hu and C. Wei, In-Situ Growth of a Bimetallic Cobalt-Nickel Organic Framework on Iron Foam: Achieving the Electron Modification on a Robust Self-Supported Oxygen Evolution Electrode, *ChemCatChem*, 2019, **11**(24), 6061–6069.

25 M. Murtaza, K. Farooq, A. A. Amjad, S. S. A. Shah and A. Waseem, Bimetallic Fe/Ni-Btc MOF Decorated Mxene

© 2025 The Author(s). Published by the Royal Society of Chemistry

Hybrid for Improved Oxidation of Water, *Diamond Relat. Mater.*, 2024, **147**, 111379.

26 Z. Zhang and H. Karimi-Maleh, Label-Free Electrochemical Aptasensor Based on Gold Nanoparticles/Titanium Carbide Mxene for Lead Detection with Its Reduction Peak as Index Signal, *Adv. Compos. Hybrid Mater.*, 2023, **6**(2), 68.

27 L. Zhao, B. Dong, S. Li, L. Zhou, L. Lai, Z. Wang, S. Zhao, M. Han, K. Gao and M. Lu, Interdiffusion Reaction-Assisted Hybridization of Two-Dimensional Metal–Organic Frameworks and $Ti_3C_2T_x$ Nanosheets for Electrocatalytic Oxygen Evolution, *ACS Nano*, 2017, **11**(6), 5800–5807.

28 X. Feng, H. Chen and F. Jiang, *In Situ* Ethylenediamine-Assisted Synthesis of a Magnetic Iron-Based Metal-Organic Framework MIL-53 (Fe) for Visible Light Photocatalysis, *J. Colloid Interface Sci.*, 2017, **494**, 32–37.

29 M. Yaghoubi, A. R. Zanganeh, N. Mokhtarian and M. H. Vakili, ZIF-67 Nanocrystals for Determining Silver: Optimizing Conditions by Box–Behnken Design, *J. Appl. Electrochem.*, 2022, **52**(4), 683–696.

30 L. Wang, Z. Wang, L. Xie, L. Zhu and X. Cao, ZIF-67-Derived N-Doped Co/C Nanocubes as High-Performance Anode Materials for Lithium-Ion Batteries, *ACS Appl. Mater. Interfaces*, 2019, **11**(18), 16619–16628.

31 A. R. Paulraj, Y. Kiros, B. Skårman and H. Vidarsson, Core/Shell Structure Nano-Iron/Iron Carbide Electrodes for Rechargeable Alkaline Iron Batteries, *J. Electrochem. Soc.*, 2017, **164**(7), A1665.

32 T. Yousaf, A. Areeb, M. Murtaza, A. Munir, Y. Khan and A. Waseem, Silane-Grafted Mxene ($Ti_3C_2T_x$) Membranes for Enhanced Water Purification Performance, *ACS Omega*, 2022, 7(23), 19502–19512.

33 P. Dinh Du and P. Ngoc Hoai, Synthesis of MIL-53 (Fe) Metal-Organic Framework Material and Its Application as a Catalyst for Fenton-Type Oxidation of Organic Pollutants, *Adv. Mater. Sci. Eng.*, 2021, **2021**(1), 5540344.

34 N. Mostafazadeh, A. Ghoreyshi and K. Pirzadeh, Optimization of Solvothermally Synthesized ZIF-67 Metal Organic Framework and Its Application for Cr(vi) Adsorption from Aqueous Solution, *Iran. J. Chem. Eng.*, 2018, **15**(4), 27–47.

35 K. Farooq, M. Murtaza, Z. Yang, A. Waseem, Y. Zhu and Y. Xia, Mxene Boosted MOF-Derived Cobalt Sulfide/Carbon Nanocomposites as Efficient Bifunctional Electrocatalysts for OER and HER, *Nanoscale Adv.*, 2024, **6**, 3169–3180.

36 L. Deng, Z. Yang, R. Li, B. Chen, Q. Jia, Y. Zhu and Y. Xia, Graphene-Reinforced Metal-Organic Frameworks Derived Cobalt Sulfide/Carbon Nanocomposites as Efficient Multifunctional Electrocatalysts, *Front. Chem. Sci. Eng.*, 2021, **15**(6), 1487–1499.

37 P. Li, Y. Xuan, B. Jiang, S. Zhang and C. Xia, Hollow La0.6sr0.4ni0.2fe0. 75MoO.05o3-Δ Electrodes with Exsolved $FeNi_3$ in Quasi-Symmetrical Solid Oxide Electrolysis Cells for Direct CO_2 Electrolysis, *Electrochem. Commun.*, 2022, **134**, 107188.

38 W. Gu, M. Wu, J. Xu and T. Zhao, Mxene Boosted Metal-Organic Framework-Derived Fe–N–C as an Efficient Electrocatalyst for Oxygen Reduction Reactions, *Int. J. Hydrogen Energy*, 2022, **47**(39), 17224–17232.

39 J. Wang and F. Ciucci, Boosting Bifunctional Oxygen Electrolysis for N-Doped Carbon *Via* Bimetal Addition, *Small*, 2017, **13**(16), 1604103.

40 M. Gao, W. Sheng, Z. Zhuang, Q. Fang, S. Gu, J. Jiang and Y. Yan, Efficient Water Oxidation Using Nanostructured A-Nickel-Hydroxide as an Electrocatalyst, *J. Am. Chem. Soc.*, 2014, **136**(19), 7077–7084.